minerals

MDPI

Article

Preliminary U-Pb Detrital Zircon Ages from Tufiti di Tusa Formation (Lucanian Apennines, Southern Italy): Evidence of Rupelian Volcaniclastic Supply

Annamaria Fornelli [1], Salvatore Gallicchio [1], Francesca Micheletti [1,*] and Antonio Langone [2]

[1] Earth Science and Geo-Environmental Department, University of Bari Aldo Moro, via E. Orabona, 4, 70125 Bari, Italy; annamaria.fornelli@uniba.it (A.F.); salvatore.gallicchio@uniba.it (S.G.)

[2] Geosciences and Earth Resources Institute (IGG-CNR)—U.O.S. of Pavia, via Ferrata, 1, 27100 Pavia, Italy; langone@crystal.unipv.it

* Correspondence: francesca.micheletti@uniba.it

Received: 5 July 2020; Accepted: 3 September 2020; Published: 6 September 2020

Abstract: U-Pb spot ages have been determined on detrital zircons from two samples of volcaniclastic arenites belonging to the Tufiti di Tusa Formation (TTF) outcropping in the Lucanian Apennines (Southern Italy). Many petrographic and geochemical studies have been performed on these sandstones with the aim of defining their detritus source. A new and precise evaluation of the mineralogical composition of metamorphic lithic fragments, together with U-Pb detrital zircon ages, helps to clarify the deposition age of these syn-sedimentary volcaniclastic sandstones and constrains their source areas. Volcaniclastic arenites consist of andesitic fragments and single minerals of plagioclases, clinopyroxenes, and hornblendes, while the metamorphic lithics are mainly fragments of blue amphibole-bearing micaschists, serpentinites, ophicalcites, phyllites, and medium-grade micaschists. Phaneritic plutonic fragments consist of quartz, feldspar, and micas. Carbonate components include biomicritic and biosparitic fragments. Eighty age data collected from 56 zircons reveal a wide age spectrum, ranging from Neoarchean to Rupelian (from 2712 ± 25 to 30 ± 1 Millions of years (Ma)). The age data show that in volcaniclastic sandstones there is evidence of ancient crystalline basements involved in Cadomian and Variscan orogenesis (ages from 2712 ± 25 Ma to ≈260 Ma), whereas the measured ages of 157 Ma testify the events of Pangea fragmentation and the ages between 78 and 67 Ma are related to subduction metamorphism connected to the Alpine orogenesis. Fifty percent of the estimated detrital zircon ages show a mean concordant age of 33 ± 1 Ma, they have been measured on idiomorphic crystals with undisturbed magmatic oscillatory zoning. These data reveal the true sedimentation age of Tufiti di Tusa sandstones at least at the sampled levels, coeval with that recorded in other Rupelian volcaniclastic successions outcropping in the Northern Apennines and in the Western Alps (e.g., Val d'Aveto-Petrignacola Formation, Ranzano Formation and Taveyannaz Sandstone). These data represent preliminary suggestions of the sedimentation age of the Tufiti di Tusa Formation and Rupelian paleogeography in the Western Mediterranean area. During Priabonian-Rupelian times, the volcanic calc-alkaline detritus linked to a widespread syn-sedimentary igneous activity on the hinterland terranes of the foredeep basins in the Apennine-Maghrebian orogen extended from north to south in the Western-Central Mediterranean area.

Keywords: volcaniclastic sandstones; Rupelian volcanism; U-Pb zircon ages; Lucanian Apennines

1. Introduction

In the Western Mediterranean area, the Alpine belt was marked by intense deformation and high pressure-low temperature metamorphism in ophiolite sequences and their sedimentary covers,

followed by retrograde tectonic phases associated with decompression and exhumation together with continental crust sectors during the Paleocene-Eocene period [1]. Successively, from the Late Eocene-Oligocene up to the Early Miocene period, a westward subduction of the Neotethys remnants and the Adria platform took place and a volcanic arc was activated in the Central-Western Mediterranean area. Consequently, syn-orogenic volcaniclastic turbidite deposits began to accumulate in the internal and external areas of the Apennine-Maghrebian foredeep basin system [2,3]. The presence of syn-sedimentary volcaniclastic deposits in the Oligocene-Miocene foredeep sedimentary units of the Apennine-Maghrebian chain (Oceanic Flysch Basin) [4,5] provides important constraints for the reconstruction of the paleogeography and tectonic evolution of the Western Mediterranean area. In fact, the geochemical and minero-petrographic characteristics of volcaniclastic detritus are a prerequisite for the recognition of the timing and location of volcanic source areas and the depositional domains in which the detritus was quickly stored. The volcaniclastic deposits are now scattered discontinuously along the Apennine-Maghrebian Chain and in the external sector of the Western Alps (Figure 1a). The oldest sedimentary records revealing coeval calc-alkaline volcanic activity during the Apennine-Maghrebian Orogen are Late Eocene - Early Oligocene in age and correspond to (Figure 1a,b): (i) The Val d'Aveto -Petrignacola and Ranzano formations in the northern inner sector of the Apennine belt, representative of the Sub-ligurian and Epiligurian domains, respectively [6–8]; (ii) volcaniclastic sandstones of the Taveyannaz Formation deposited in the north Alpine foreland basin within the external sector of the Western Alps [9]. The remnants of these deposits rest along the Periadriatic faults in the Alps, in SE France, in the Sardinia-Corsica Region, and in the Northern Apennines [6,9–11]. In the Southern Apennine-Maghrebide chain, the coeval foredeep deposits, instead, are represented by argillaceous and calcareous turbidites with minor micaceous sandstones [12–14]. Only in the Early Miocene did huge amounts of syn-sedimentary volcaniclastic detritus accumulated in southern orogenic system (Figure 1b), recorded by the Tufiti di Tusa Formation (TTF) characterizing the upper part of the Sicilidi Units (Troina-Tusa Unit, in Sicily and the Rocca Imperiale Unit in the Calabria and Basilicata Regions) [15]. However, the deposition age of the TTF is still debated in literature. The classic biostratigraphic methods indicate a Late Oligocene–Early Miocene age [14,16–18], whereas a Late Eocene-Early Oligocene age has been indicated by [19], on the basis of well-documented calcareous nano-fossil and palynomorph assemblages.

With the aim of elucidating the paleogeographic context and the sedimentation age of TTF volcanic detritus and to evaluate their timing and genetic relationships with potential source areas, U-Pb detrital zircon ages from two samples of volcaniclastic sandstones were considered to date this depositional event and to evaluate the relationships with other volcaniclastic deposits outcropping in the Northern Apennines and the Western Alps. The volcaniclastic deposits as expression of syn-sedimentary volcanic activity, are promising for this purpose. In addition, a reassessment of the lithic fragment paragenesis from sandstones can provide new geological pieces for the reconstruction of the provenance area puzzle related to the paleogeography of Apennine foredeep basins that form the Southern Apennine chain.

Geochronological approaches regarding volcaniclastic sediments of the TTF are missing, consequently, the collected U-Pb detrital zircon ages are the first absolute ages available in the Southern Apennines.

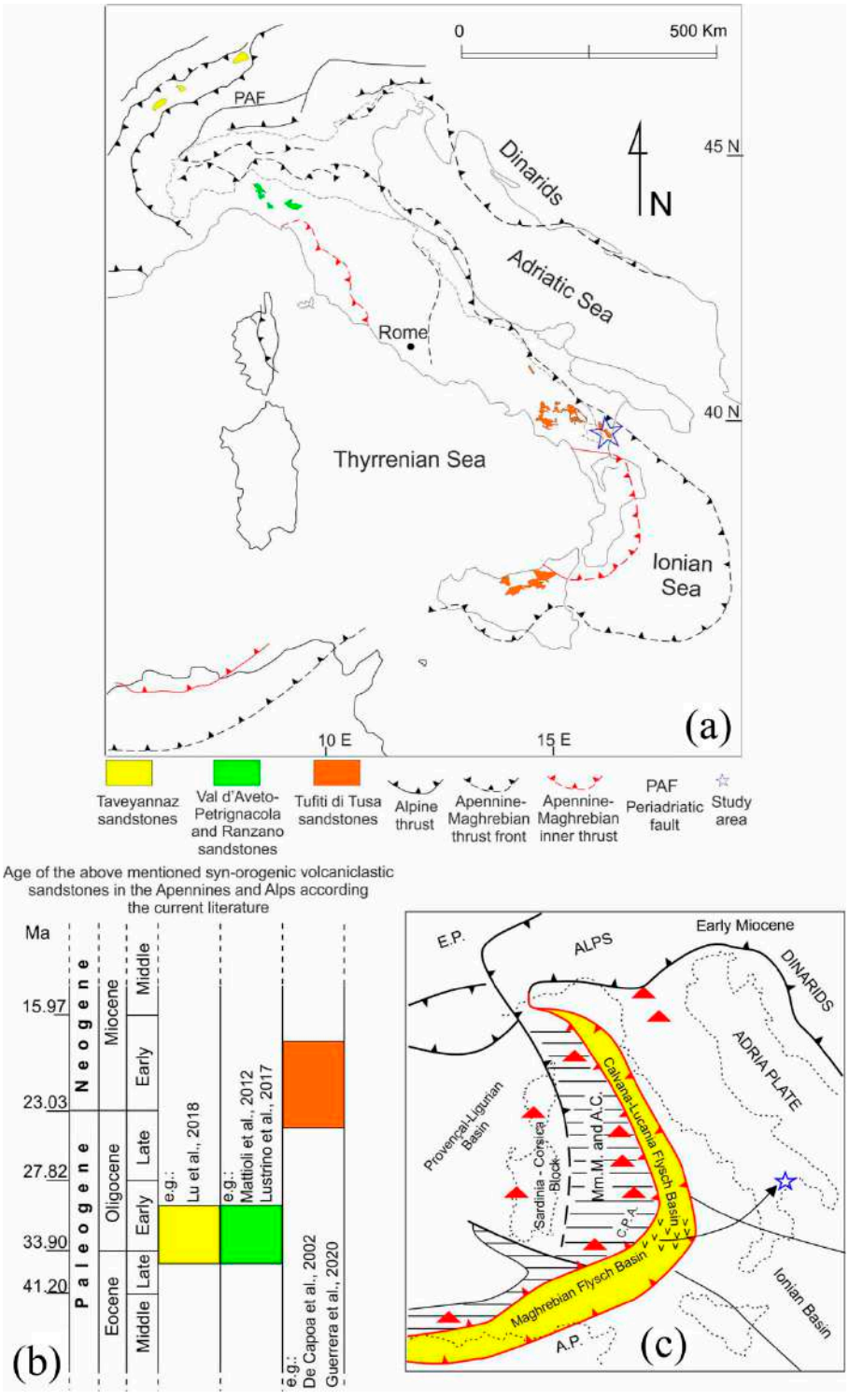

Figure 1. (**a**) Distribution of the main volcaniclastic turbidite deposits in the northern external sector of the Western Alps, in the inner sector of the Northern and Southern Apennines and in Sicily (Italy). The blue star indicates the study area. (**b**) Age of the above-mentioned volcaniclastic sandstones according to the current literature. (**c**) Paleogeographic and paleotectonic sketch of the Apennine-Maghrebian foredeep basin system in the Western-Central Mediterranean area in the Early Miocene. Symbols "vvv" represent the depositional domain of volcaniclastic sandstones; blue star is the geographical location of the studied outcrops (modified from [2,20]). Mm.M., Mesomediterranean Microplate; A.C., Alpine Chain; E.P., European Plate; A.P., African Plate; C.P.A., Calabria-Peloritani Arc.

2. Geological Framework of Volcaniclastic Detritus

The Apennine belt extending from north to south along the Italian peninsula, represents one of the younger orogenic systems in the circum-Mediterranean area, and it is still active in the Ionian Sea [2,21–23]. Its tectonic evolution took place in the Western Mediterranean area, owing to the interaction between the lithospheric plates belonging to European and African domains. The ancient tectonic elements of the Apennine chain (Figure 1c) are related to the westward subduction of oceanic, transitional, and continental lithosphere belonging to the remnant northern-western Neotethys or the east Ligurian Tethys, located on the western side of the Adria Plate [2,24]. The hinterland domain of this tectonic system is represented by the European Sardinia-Corsica block and other smaller continental microplates, generally grouped in the Mesomediterranean Microplate (Figure 1c) [17,20]), formed by Cadomian, Variscan, and Alpine fragments, including rocks of continental and oceanic origin (Variscan granitoids, low- middle- and high-grade Variscan metamorphites, and Alpine ophiolites). Calc-alkaline volcanic activity developed both in internal [10,18–20,25] and in foreland domains [26]. On this subducting system, deep marine foredeep basins developed, known from the north to the south as the Sub-ligurian and Sicilidi domains or as the Calvana-Lucania and Maghrebian Oceanic Flysch basins [17] developed (Figure 1c). The remnants of these basins are now scattered from the Alps to the Southern Apennine-Maghrebian chain. They consist of turbiditic deposits containing volcaniclastic detritus derived from a syn-sedimentary magmatic activity [27–31]. The different ages of volcaniclastic sandstones from the Alps and the Northern Apennines (Late Eocene-Early Oligocene) to the Southern Apennines (Lower Miocene) are linked to the migration of the volcanic activity, presumably due to the subduction plain roll-back [25]. However, determining the deposition age of the volcaniclastic sandstones in the Southern Apennines is a crucial challenge to be solved. Was the volcaniclastic detritus deposited later in the Southern Apennines than in the northern sectors? Was the volcanic activity of the Sardinia-Corsica block similar to that of the Mesomediterranean Microplate?

The turbidite deposits of deep marine foredeep basins are well represented in the external sector of the Southern Apennines near the Ionian Coast (Figure 1a). In this sector of the chain, the Rocca Imperiale Tectonic Unit belonging to the Sicilide Complex crops out (Figure 2) [16,32]. This tectonic unit is regionally subdivided into two tectonically superimposed sub-units (Figure 2), represented from top to bottom by the Torrente Cerreto sub-unit and the Corleto Perticara sub-unit. The Torrente Cerreto sub-unit shows a chaotic structure typical of a tectonic mélange, in contrast, the sedimentary succession of the Corleto Perticara sub-unit is well preserved and consists, from bottom to top, of the following formations (Figure 3): Argille Varicolori Inferiori (Cretaceous-Paleocene), Monte Sant'Arcangelo Formation (Paleocene-Eocene), Argille Varicolori Superiori (Eocene-Oligocene), and TTF (Late Oligocene–Early Miocene) [32,33].

The study samples derive from a stratigraphic section located to the west of Rotondella Village (Matera district) along the valley of Candela Stream (Figure 3a,b), where the Sicilidi units are represented by the younger formations of the Corleto Perticara tectonic sub-unit: The Argille Varicolori Superiori and the TTF (Figure 3b,c). These units overthrust regionally the Nova Siri Tectonic Subunit (NSTS), represented mainly by the external Lower-Middle Miocene turbidite units of the Flysch Numidico and the Serra Palazzo formations ([34,35] (Figure 3c). Toward the east, the Corleto Perticara tectonic subunit, representing the outcropping front of the chain, is unconformably covered by the Plio-Pleistocene sandy and clayey Bradanic Trough deposits (BTDs) [21,32].

The TTF formation lies unconformably on the Argille Varicolori Superiori and outcrops at the core of a syncline structure (Figure 3b). From a lithostratigraphical point of view, the formation is represented by a turbidite sedimentary succession, approximately 250 m thick, varying from calciclastic to grey-green siliciclastic-volcaniclastic arenites interbedded in mudrocks. In particular, the large amount of the volcaniclastic detritus characterizes the uppermost 60 m of the succession [33,36]. The observed sedimentary structures at the bottom of the volcaniclastic strata correspond to flute and load casts, indicating the prevalent southern provenance direction of detritus [28,36–38] in the current geographical location. If the anticlockwise rotation of several tens of degrees of the Southern

Apennines toward the Adria plate is taken into account [39,40], the southern provenance directions becomes almost western (Figure 1c).

Two samples, namely, TTA and TTB (Figure 3b,c), of volcaniclastic sandstones belonging to the upper part of the TTF were considered for their petrographic, chemical, and geochronological characteristics. The TTA sample (40°09′46.80″ N–16°29′29.42″ E) is representative of grey coarse-grained sandstones, whereas the TTB sample (40°09′55.75″ N–16°29′38.09″ E) shows fine-grained texture and derives from greenish portions.

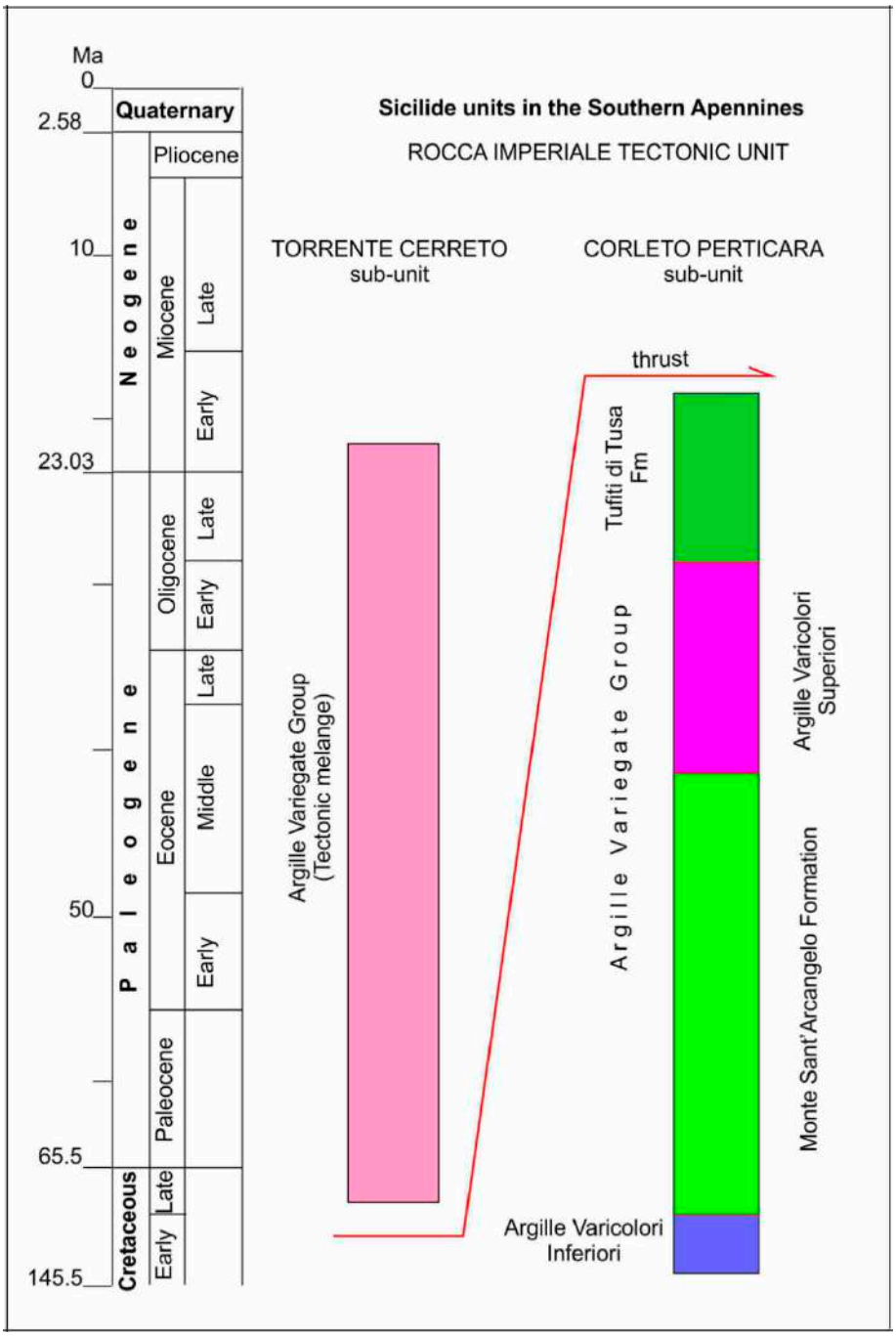

Figure 2. Schematic stratigraphic features of the Sicilidi units in the study area (modified from [32]).

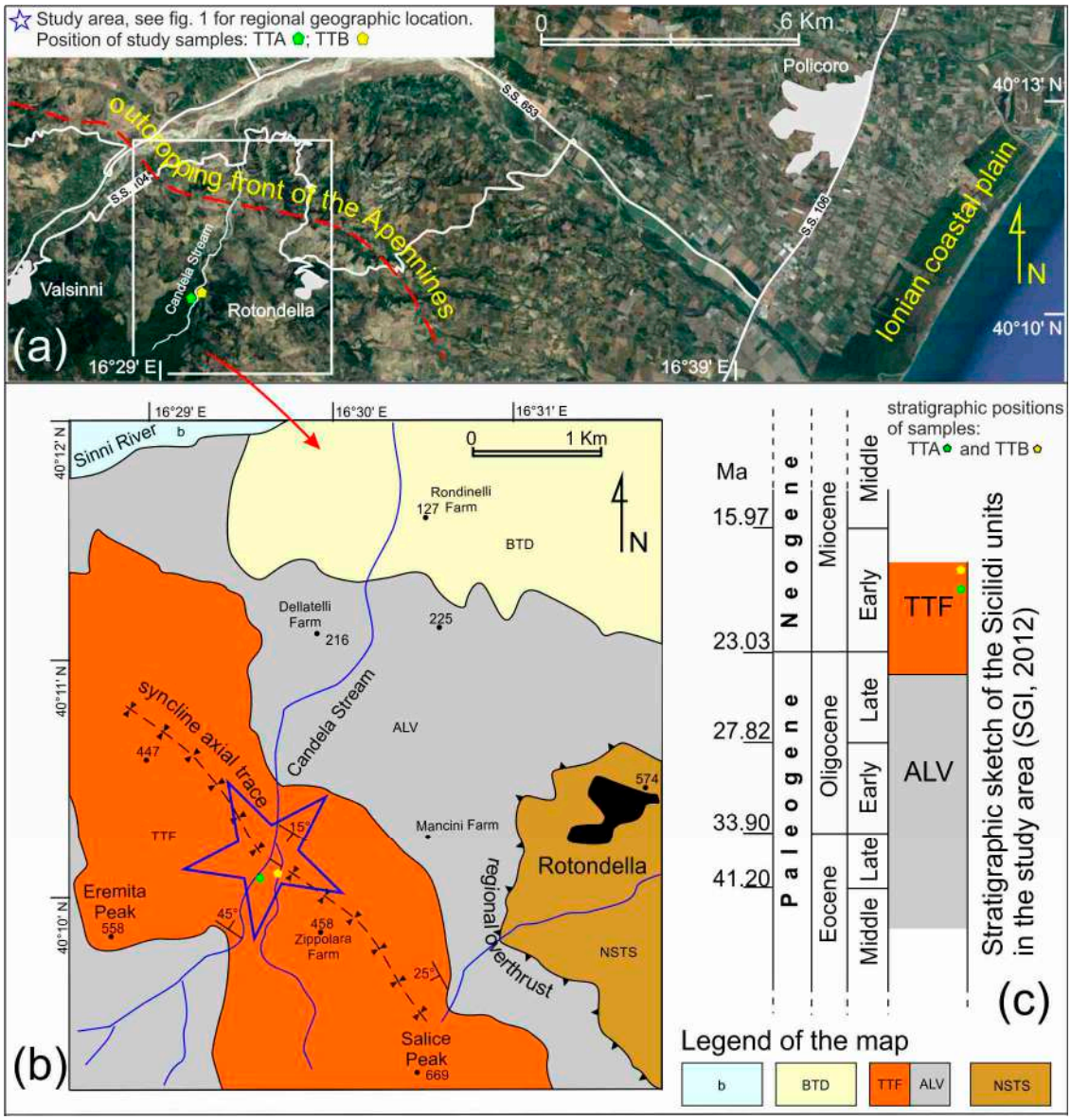

Figure 3. (**a**) Study area, modified from Google Earth. (**b**) Geological map of the study area, modified from [33]. (**c**) Stratigraphic sketch of the Sicilidi units in the study area modified from [32] showing the stratigraphic position of the study samples. NSTS, Nova Siri Tectonic Subunit (Cretaceous–Middle Miocene); ALV, Argille Varicolori Superiori Formation (Middle Eocene–Late Oligocene); TTF, Tufiti di Tusa Formation (Late Oligocene–Early Miocene); BTD: Bradanic Trough Deposits (Middle Pliocene Pleistocene); b, Alluvial deposits (Late Pleistocene-Olocene).

3. Analytical Methods

Modal analyses were performed under an optical microscope on two samples of TTF sandstones with the aim of verifying if their petrographic composition is similar to that already known in the literature [28,31,37,38]. Point counts were made following the Gazzi-Dickinson method [41,42]; approximately 500 points were counted on each thin section, distinguishing the single crystalline phases by fine-grained fragments. The proportions of total quartz (Q), feldspar (F), and fine-grained lithic fragments (L) for plotting a QFL diagram were obtained by recalculation of 100% of the analytical data.

Major and various trace element analyses of the whole rock were performed by FRX utilizing a Philips PW1480 automatic spectrometer (Earth Science and Geo-environmental Dep., University of Bari, Italy) to determine the chemical composition of the volcaniclastic detritus and to compare it to

that known in the literature. The samples were promising for zircon selection, the Zr content being 145 and 166 ppm in the TTA and TTB samples, respectively.

Detrital zircon crystals were extracted from 50–125 μm and 125–250 μm fractions obtained from approximately 3 kg of rock. The finer fraction (50–125 μm) was more fertile for zircons in both samples, but the medium-coarse-grained fraction was almost promising in the coarse-grained sample (TTA). The small and big zircons were selected for U-Pb dating with the aim of evaluating the possible dependence of the zircon ages from the particle sizes [43,44]. More steps with the Frantz magnetic separator were needed to remove all quartz grains wrapped by oxidation patina. Subsequently, the non-magnetic fractions were treated with a high-density solution for gravity separation.

The clearest, internal crack-, and inclusion-free zircon grains were hand-picked under a stereo-microscope in order to exclude any zircons producing discordant ages not suitable for the purpose of this work [45,46]. In fact, crystals with evident radiation damage and showing metamict rims are prone of producing discordant ages [44]. After accurate selection of promising zircon grains, they were placed into epoxy resin mounts and polished to expose the grain interior.

Analysis of the morphology and internal micro-textures of the zircons was performed using scanning electron microscope (SEM) using a Zeiss EVO50XVP (at University of Bari).

Backscattered electron detector (BSED) images were used to examine morphologic features and to check inclusion and fracture occurrence. Internal zoning patterns were evidenced by a variable pressure secondary electron (VPSE) detector, settled under high-vacuum conditions, which revealed high-resolution images perfectly comparable to the most common cathodoluminescence images [47]. The VPSE images were very useful for determining the location of spots on homogeneous crystal domains that were suggestive of a clear origin of the detrital zircons. After geochronological investigation, the zircon grains were further inspected with the VPSE detector, to check the precise location of the ablated spots.

U-Pb spot analyses were performed by LA-ICP-MS at the IGG-CNR (Pavia, Italy) utilizing the system configuration and methodology reported by [48,49]. For details about the analytical setting, refer to [50,51]. All analytical results are shown in Supplementary Table S1.

The data reduction, age calculation, and uncertainty propagation were performed following [52,53]. The filtering of the U–Pb ages was mainly based on a 10% cut off of the discordance of the given $^{206}Pb/^{238}U$ age for zircons with ages younger than 1.4 Ga. Instead, for grains older than 1.4 Ga, the $^{206}Pb/^{207}Pb$ age was considered as the best age in dependence of minor error of this ratio linked to Pb loss in inherited zircons [52,53]. The representation of age data follows the model of kernel density estimation [54].

4. Petrographic and Chemical Features of Sandstones

4.1. Background

Previous works [18,28,31,37,38] have exhaustively detailed the petrographic and geochemical aspects of TTF sandstones outcropping along the Southern Apennines. Three distinct petrofacies were recognized in [37]: (i) feldspatolithic sandstones; (ii) quartzose sandstones; (iii) volcanolithic sandstones. According to [28,31] from the bottom to the top of TTF four petrofacies can be distinguished: (i) quartzolithic sandstones; (ii) lithofeldspatic-volcaniclastic sandstones; (iii) lithofeldspatic sandstones with dominant volcanic detritus; (iv) feldspatolithic sandstones with abundant volcanic component.

The upper part of the arenaceous succession contain abundant volcaniclastic detritus as single minerals or porphyritic andesite lithics, peculiar metamorphic lithics such as serpentinites, blue amphibole-bearing micaschists, garnet-bearing micaschists, epidote-bearing micaschists, orthogneisses and single heavy minerals as staurolite, glaucophane, epidote, and garnet. The blue amphibole is mainly crossite and subordinately glaucophane, and it coexists with albite, quartz, phengite, epidote, garnet and titanite, indicating that high-pressure metamorphic rocks were present among the source

rocks [37]. The chemistry of whole rocks allowed to classify the volcanic material as andesitic, consistent with the nature of the volcanic lithics and single crystals [37].

An accurate mineralogical characterization of the interbedded mudrocks together with detrital grain features suggested poor sorting related to rapid sedimentation without significant recycling processes [31]. Further evidence of the volcaniclastic nature of the supply emerged from volcanic glass shards found in thin mudrock levels and from the abundance of smectite in the Illite/Smectite (I/S) mixed layers, probably related to the diagenetic alteration of the weathered original pyroclastic and/or volcaniclastic rocks [31].

4.2. Sample TTA and TTB

The selected sandstones derive from feldspatolithic petrofacies as indicated by [28,31]. The TTA sample is representative of medium-coarse-grained sandstones and the TTB sample of fine-grained types. The petrographic composition of the two samples is comparable, despite different grain size (Figure 4a,b), and both predominantly contain angular fragments, scarce cement, and a pseudo-matrix derived from the alteration of volcanic components. The fine-grained sample (TTB in Figure 4b) contains more abundant alteration products in pseudo-matrix due to its fine-grained texture. The principal composition is in average Q_{16} F_{52} L_{32} and the framework consists of prevalent volcanic detritus (approximately 70% in volume) represented by single minerals and porphyritic andesite lithics with phenocrysts of zoned plagioclase, clinopyroxene and brown/green amphiboles (Figure 4c,d). Granitic, metamorphic, siliciclastic, and carbonate components are present in minor amounts. The phaneritic plutonic fragments consist of quartz, feldspar, and micas (Figure 4a). Among the metamorphic lithics, low- and medium-grade micaschists, orthogneisses, ophicalcites, and serpentinites (Figure 4e,f) are evident together with blue amphibole-bearing micaschists (Figure 4g,h). Single crystals of mica, feldspar, quartz, epidote, staurolite, garnet, and blue amphibole are widespread, together with biomicritic and biosparitic fragments.

The chemical compositions of study sandstones (Table 1) are comparable showing high contents of Fe_2O_3 (around 7 wt%) and MgO (5.5 wt% on average), compatible with the prevalent intermediate mafic character of detritus associated with a low content of Rb and high Sr values related to abundant volcanic An-rich plagioclase. The slightly higher Al_2O_3 and Sr contents and lower MgO and Fe_2O_3 values in the TTB sample with respect to TTA could be related to a more intense alteration of the first.

Table 1. Chemical composition of TTA and TTB samples and the mean of chemical composition of the volcaniclastic sandstones reported in [37]. Trace elements are expressed in ppm.

Sample	SiO_2	TiO_2	Al_2O_3	Fe_2O_3	MnO	MgO	CaO	Na_2O	K_2O	P_2O_5	LOI	Rb	Sr	Y	Zr	Nb
TTA	52.94	0.69	16.55	7.40	0.08	5.67	5.33	2.23	1.32	0.10	7.68	43	597	20	145	11
TTB	54.08	0.72	18.00	6.71	0.09	5.23	4.58	2.82	1.63	0.15	6.00	55	960	19	166	11
Mean in [37]	54.37	0.77	15.19	6.72	0.09	5.36	6.00	2.96	1.68	0.15	6.34	63	724	21	146	9

LOI: loss on ignition.

In Figure 5, the principal composition of the study samples is compared to the literature data [18,28,31,37,38] in the Dickinson's provenance diagram [55]. They fall into the same field, corresponding to feldspatolithic sandstones with abundant volcanic components named petrofacies iv [28,31]; in addition, the detrital mode of these sandstones is related to a magmatic arc source [55,56]. A comparison with the chemical composition of volcaniclastic sandstones reported by [37] (Table 1) confirms that the study samples show a composition very similar to feldspatolithic sandstones with abundant volcanic component.

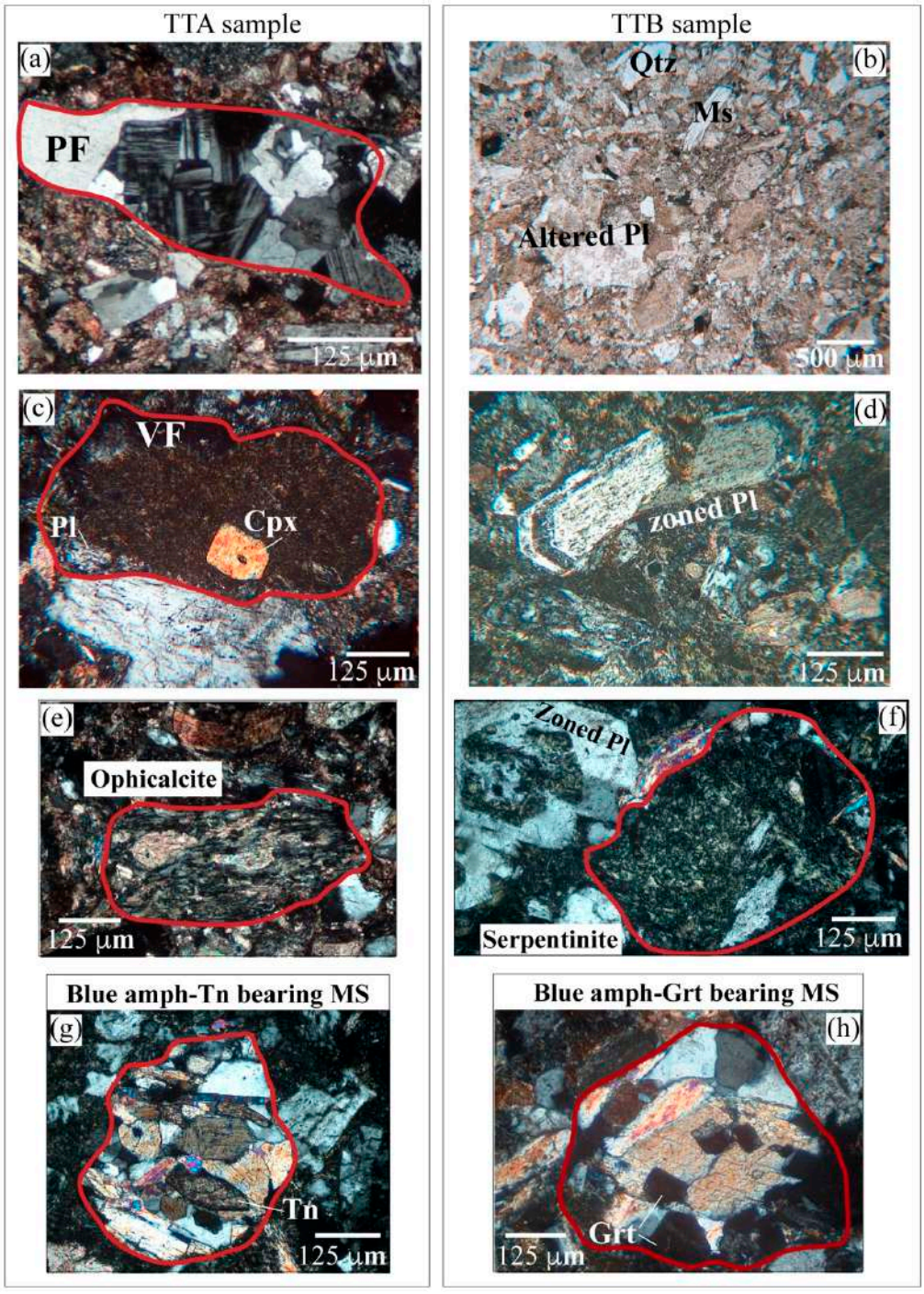

Figure 4. Microphotographs of the coarse-grained TTA sample (to the left): (**a**) granitic fragment, (**c**) volcanic fragment with phenocrysts of plagioclase and clinopyroxene; (**e**) ophicalcite fragment; (**g**) blue amphibole-bearing micaschist with titanite. Microphotographs of fine-grained TTB sample (to the right): (**b**) abundant pseudo-matrix; (**d**) volcanic zoned plagioclase and alteration products in pseudo-matrix; (**f**) serpentinite fragment; (**h**) blue amphibole-garnet-bearing micaschist. Abbreviations: PF, plutonic fragment; VF, volcanic fragment; Ms, muscovite; Pl, plagioclase; Qtz, quartz; Tn, Titanite; Grt, Garnet; MS, micaschist.

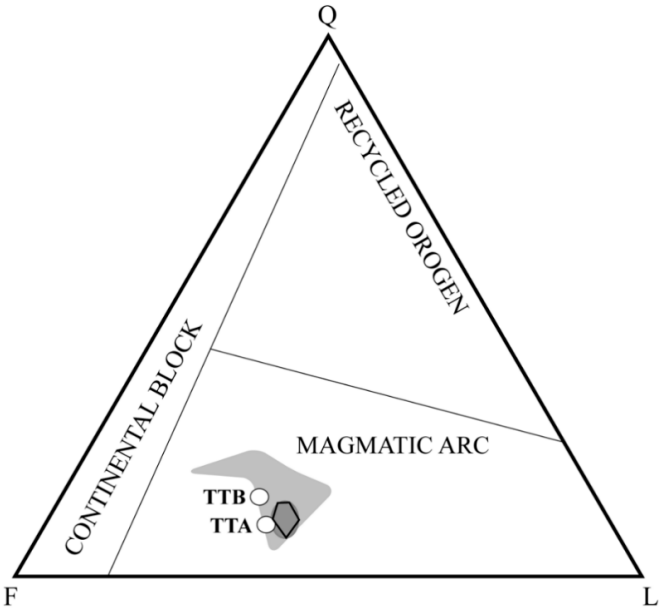

Figure 5. QFL triangular diagram with provenance indications [41,55,56]. The detrital mode of study samples TTA and TTB is compared to the literature data: light grey area [37,38]; black polygon [28]; dark grey oval [31]. Q, (total quartz); F, (feldspars); L, (fine-grained lithic fragments).

5. Morphology and Internal Zircon Textures

Fifty-six zircon crystals were separated (forty-five for the TTA sample and eleven for the TTB sample) and observed by the VPSE detector to inspect their morphological features and internal textures. Generally, the VPSE images of zircon grains show light and dark regions corresponding to lower and higher U contents, respectively. High-U dark regions usually report major radiation damages resulting from metamict zircons losing radiogenic Pb and producing discordant ages [43,53,57]. These domains were excluded for isotopic analysis.

In the realm of the selected zircons, some grains show rare fractures (zrns 36 and 6 in Figure 6a and zrn 1 in Figure 6b in the TTA sample and zrn 21 in Figure 7 in the TTB sample) or are broken with missing edge domains (zrns 4, 7 and 26, in Figure 6a,c in the TTA sample, and zrn 24 in Figure 7 in the TTB sample). These damages may have been produced during the zircon selection procedures or during the sediment transport; the preserved domains of these crystals were dated. The other selected zircon grains show euhedral-sub-euhedral habitus (e.g., zrns 6, 40, and 52C in Figure 6a and zrns 21 and 23A in Figure 7) or sub-rounded shapes (zrns 38B, 71C and 8 in Figure 6a,c,d and zrns 12 and 14 in Figure 7). Both typologies of crystals, equally distributed in the samples were dated.

The majority of the selected crystals shows an easily recognizable oscillatory zoning growth with a clear magmatic origin [50]. Best shielded magmatic zoning is evident in the preserved euhedral crystals, in which oscillatory bands can be observed in continuity from the core to the rim indicating a regular growth in a single magmatic event (zrns 45, 46, 36, 52C, 56A and 6 in Figure 6a). A few of the crystals show a sector zoning (e.g., zrn 67 in Figure 7), probably connected to changes in the rapid kinetic factor [58].

Rounded crystals with perturbed, convoluted, and blurred original concentric oscillatory zoning (zrns 58A and 30 in Figure 6b,e and zrns 14 and 17 in Figure 7) are also present; such textures can be produced by secondary modifications (i.e., post-magmatic cooling or medium-high-grade metamorphism) [50]. Sometimes they are present as inherited core domains partially reabsorbed and enveloped by successive overgrowth truncating their original zoning (e.g., zrn 44 in Figure 6e and zrn 22 in Figure 7). The great diversity of the morphology and internal pattern zoning of the zircons highlights the variety of the detrital supply, which denotes the complex and long-lasting petrogenetic history of the source rocks (i.e., igneous, metamorphic, sedimentary).

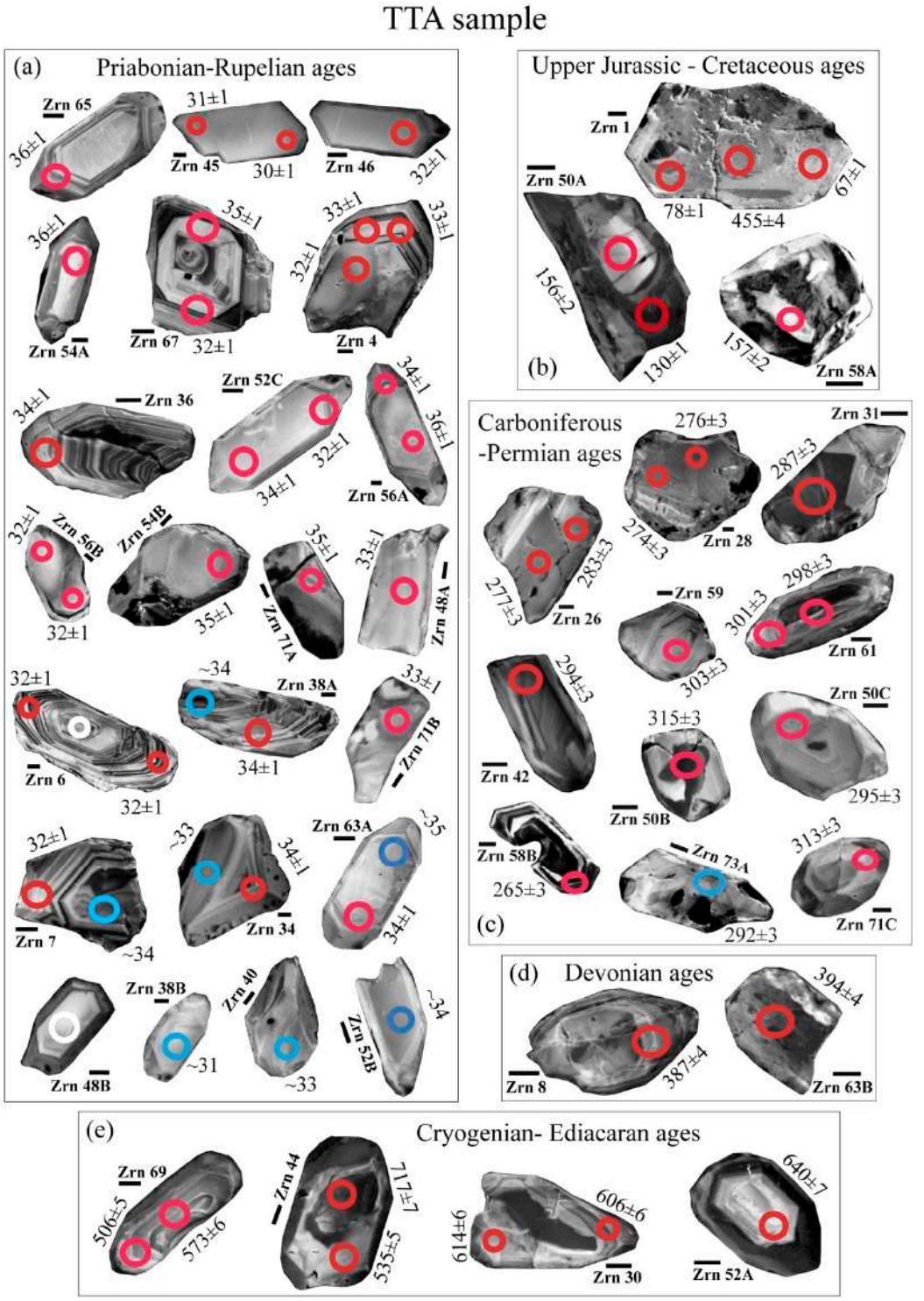

Figure 6. Variable pressure secondary electron (VPSE) images of the dated zircons in the TTA sample with spot locations and measured ages in millions of years (Ma). Red and blue circles indicate the spot location of the $^{206}Pb/^{238}U$ ages with % U-Pb discordance <±10% and those between 10% and 20%, respectively. White circles indicate the discordant ages. (**a**) Priabonian–Rupelian magmatic zircons; (**b**) Cretaceous ages at the rims of zrn1 with an Ordovician core and at the rim of zrn50A grain; Upper Jurassic ages at cores of zrn50A and zrn58A grains; (**c**) Carboniferous–Permian ages; (**d**) Devonian ages; (**e**) Cryogenian–Ediacaran ages. The notches near the crystal label refer 20 μm.

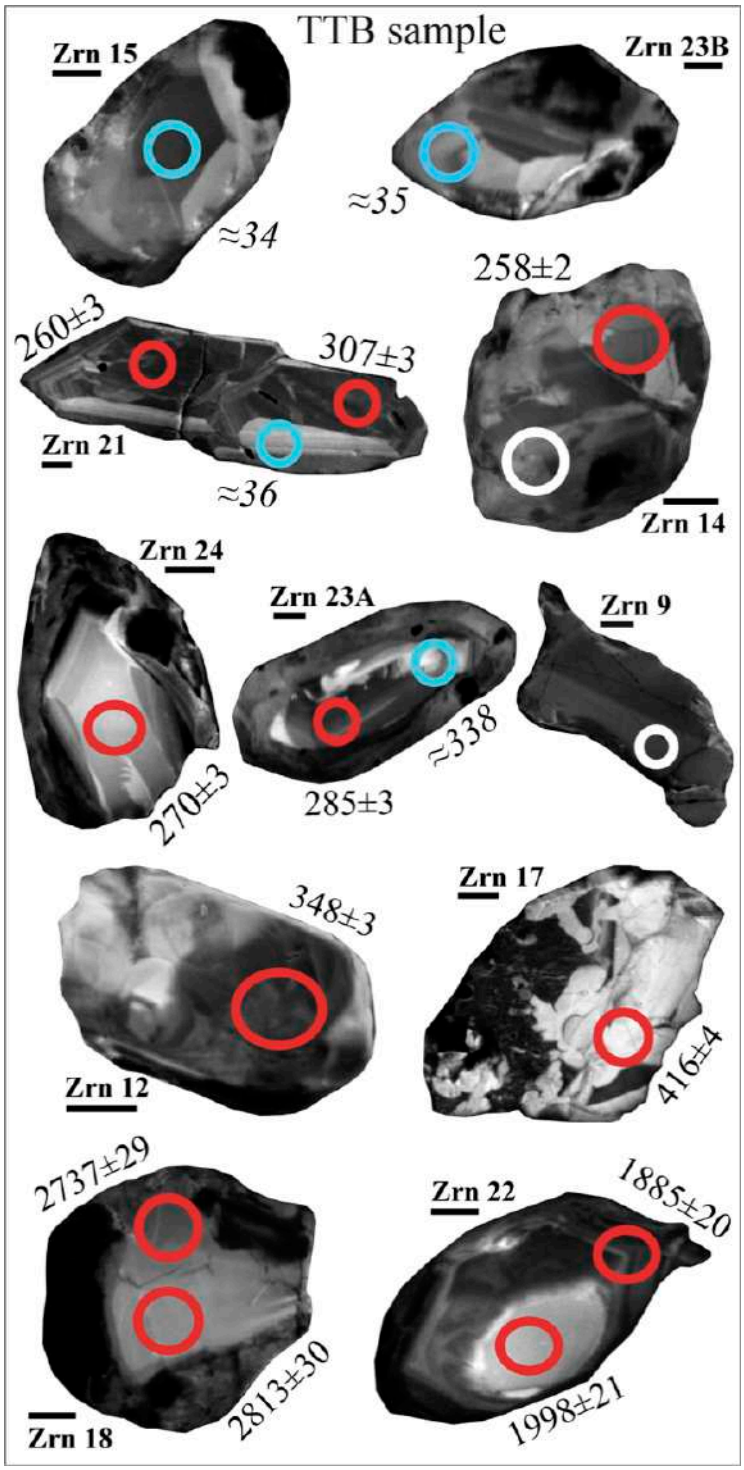

Figure 7. VPSE images of the dated zircons in the TTB sample. Red and blue circles indicate the spot location of the $^{206}Pb/^{238}U$ ages with % U-Pb discordance <±10% and those between 10% and 27%, respectively. White circles indicate the discordant ages. The ages > 1.4 Ga in zrn18 and zrn22 derive from the $^{206}Pb/^{207}Pb$ ratios. Other symbols are as described in Figure 6.

6. Detrital Zircon Chronology

The size and shape parameters of each dated zircon were measured by calculating the equivalent spherical diameter (ESD) in order to explore the potential age-size relationships. ESD is the cube root of the product of the lengths of the three axes of zircon grains; in thin sections the intermediate axis

was taken as short axis [43]. Figure 8 highlights that the distribution of ages is independent of the ESD shape parameter; in both samples, big and small grains show overlapping ages and consequently, the calculated zircon ages are representative of the whole rock. The measured zircon ages in the TTA sample are more abundant than those in the TTB sample; however, in the latter sample, records of older zircons are represented by ages ranging from 1.8 Ga to 2.8 Ga ($^{207}Pb/^{206}Pb$ ages) that were not present in the TTA sample (Figures 9 and 10).

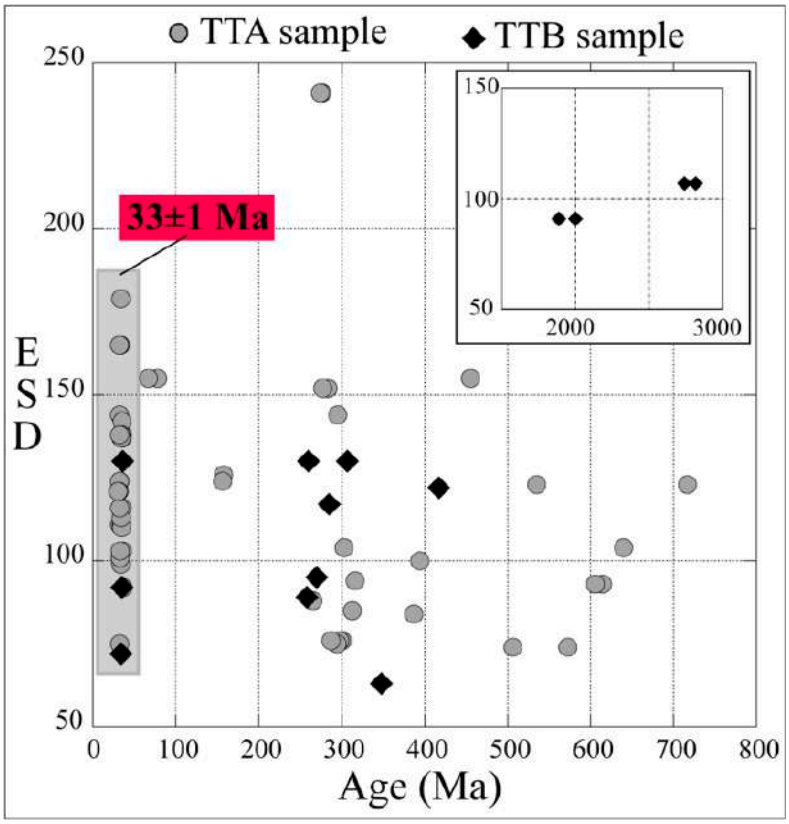

Figure 8. Equivalent spherical diameter (ESD μm) of the detrital zircon grains vs. the U-Pb ages in the TTA and TTB sandstone samples. The distribution of ages is independent from the grain-size of zircons. Ages > 1.4 Ga in TTB sample derived from the $^{206}Pb/^{207}Pb$ ratios (inset of figure).

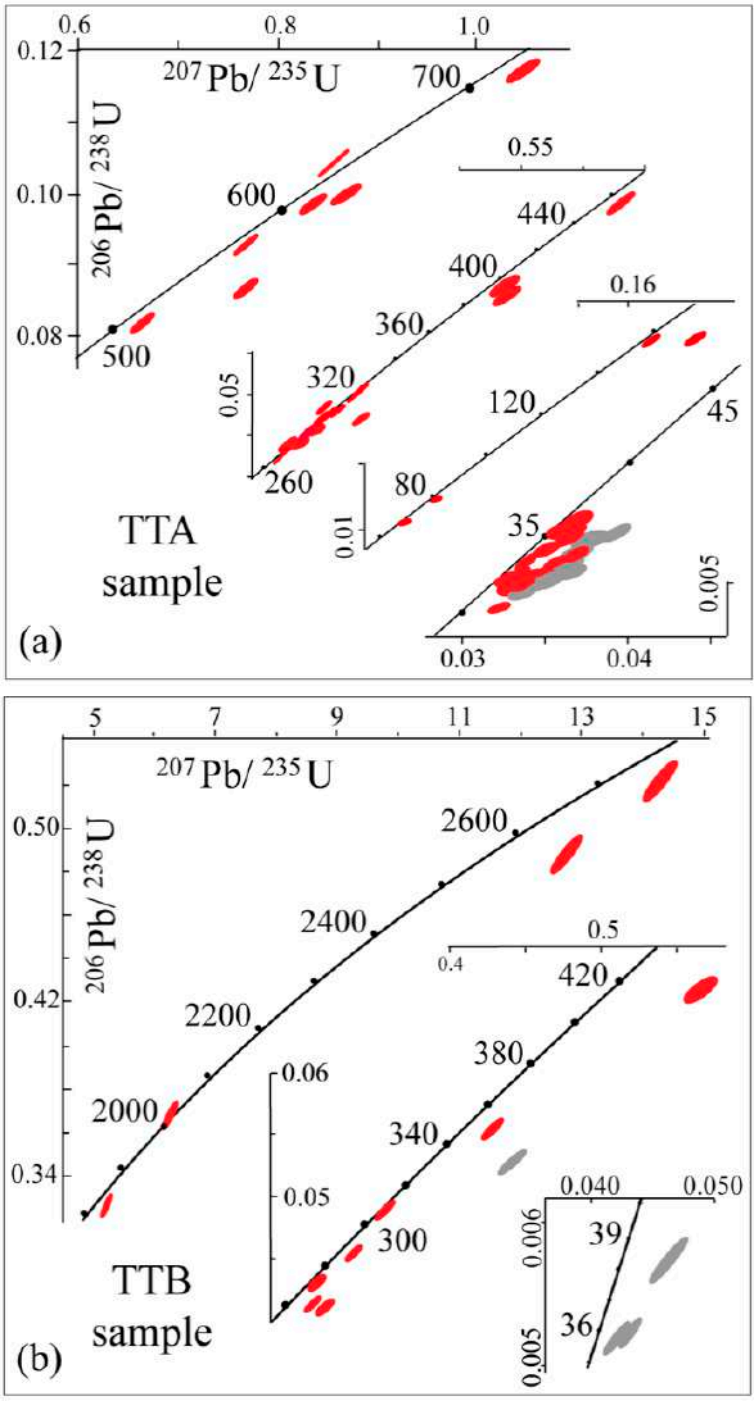

Figure 9. Concordia plot of the U-Pb ages in the TTA (**a**) and TTB (**b**) samples. Ellipses represent the ages with 2σ uncertainties. Red ellipses: Ages with % U-Pb discordance <±10%; grey ellipses: Sub-concordant ages with % U-Pb discordance comprised between 10% and 27%.

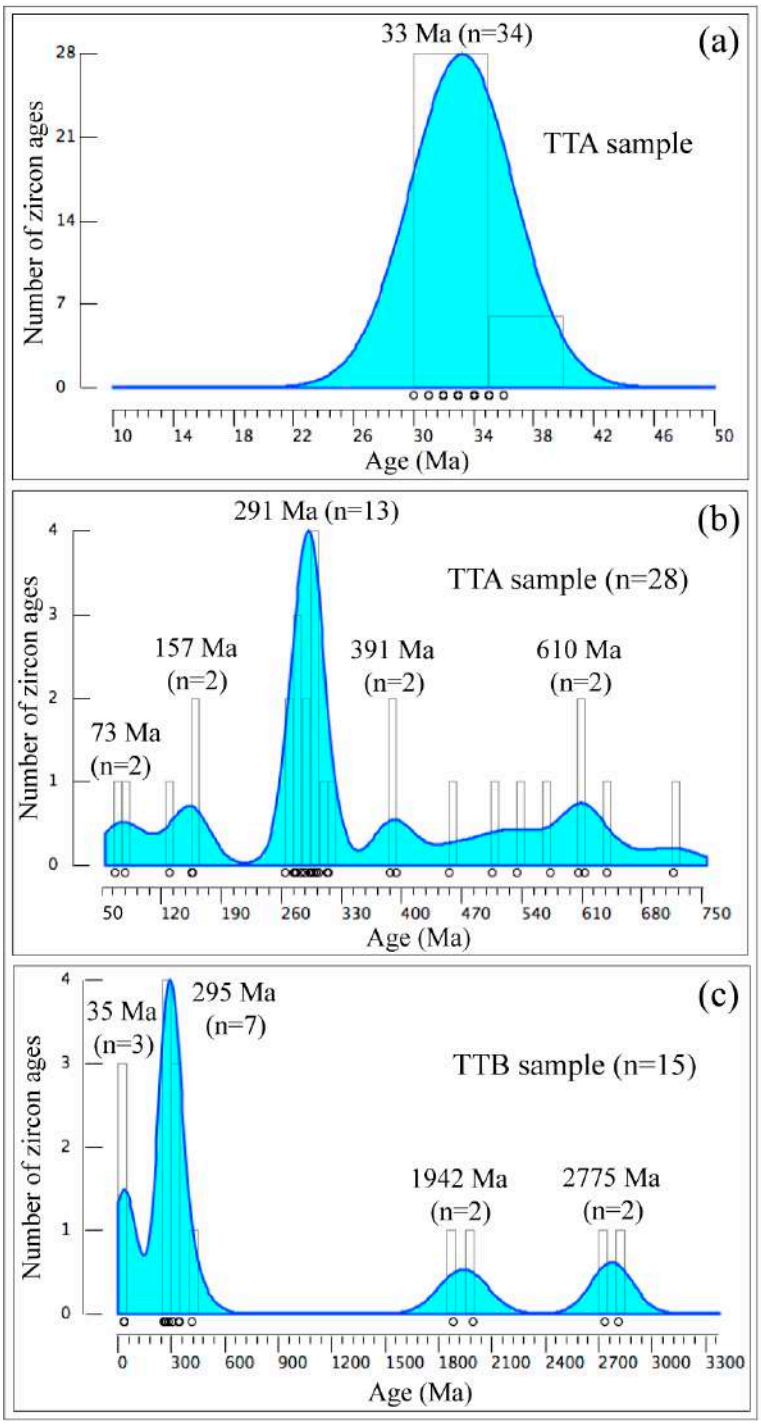

Figure 10. Histogram with Kernel density estimates [54] of the U-Pb zircon ages from the TTA (**a**,**b**) and TTB (**c**) samples. (**a**) Peak of the Priabonian-Rupelian ages in the TTA sample at 33 Ma; (**b**) pre-Cretaceous ages with peaks at 73 Ma, 157 Ma, and 291 Ma and those of pre-Devonian ages in the TTA sample.

6.1. Zircon Ages in the TTA Sample

Sixty-six U-Pb spot analyses on 45 zircon crystals yielded fifty-four concordant ages, seven sub-concordant, and five discordant data. The range of measured ages is very large, varying from 717 Ma to 30 Ma (Figures 6, 9a and 10a,b); in the following, age groups are presented by the youngest to oldest.

Half of the concordant data (50%; 27 ages) and the totality of the sub-concordant ages (seven sub-concordant ages with % U-Pb discordance <20%) range from 36 ± 1 Ma to 30 ± 1 Ma (Figures 6a, 9a and 10a), the majority of which were estimated on well-preserved idiomorphic crystals (zrns 65, 45, 46, 54A, 52C, 56A, 6, and 63A) or sometimes on broken grains (zrns 4, 36, 71A, 71B, 7, and 34) (Figure 6a). The internal textures of these crystals (i.e., idiomorphic and broken grains) show oscillatory zoning patterns typical of magmatic growth conditions even in a single crystallization event.

Three concordant Cretaceous ages at 78 ± 1 Ma, 67 ± 1 Ma, and 130 ± 1Ma were yielded on two grain envelopes (zrns 1 and 50A in Figure 6b) with perturbed oscillatory zoning domains growth on older cores dated at 455 ± 4 Ma and 156 ± 2 Ma, respectively.

Two concordant ages referable to Upper Jurassic at 157 ± 2 and 156 ± 2 Ma (zrns 50A and 58A in Figure 6b) were discovered on two corroded and modified domains showing high luminescence.

Thirteen Carboniferous-Permian ages ranging from 319 ± 3 to 265 ± 3 Ma represent the second largest group (24% of the age data; e.g., zrns 26, 28, 31, and 42 in Figure 6c); these ages are relative to the rhythmic or oscillatory zoning domains of broken grains showing a rounded shape.

Three Ordovician-Devonian ages (455 ± 4 Ma on zrn 1 in Figure 6b; 394 ± 4 Ma on zrn 63B and 387 ± 4 Ma on zrn 8 in Figure 6d) were detected on domains preserving a ghost magmatic zoning (zrn 8) or modified core domains (zrns 1 and 63B).

Seven Neoproterozoic-Cambrian ages ranging from 717 ± 7 Ma to 506 ± 5 Ma were collected in four crystals preserving sub-idiomorphic shapes (zrns 69, 44, 30, and 52A in Figure 6e). The oldest age (717 ± 7 Ma) was measured on a relict reabsorbed core showing a luminescent overgrowth dated at 535 ± 5 Ma (zrn 44 in Figure 6e). Another five ages (506 ± 5, 573 ± 6, 606 ± 6, 614 ± 6, and 640 ± 7 Ma) were detected on three crystals showing an almost well-preserved magmatic oscillatory zoning (Figure 6e).

6.2. Zircon Ages in the TTB Sample

Eleven zircon grains were analyzed in this sample and 17 spot analyses were performed. The collected data cover 11 concordant ages, four sub-concordant ages, and two discordant ages. Considering both the concordant and sub-concordant data, a large range of ages extending from 2813 ± 30 Ma to 34 ± 1 Ma were measured (Figures 7, 9b and 10c).

The youngest ages revealed in this sample were sub-concordant (% U-Pb discordance between 18% and 27%) corresponding to 34, 35, and 36 Ma. These sub-concordant ages were produced on the domains of magmatic oscillatory zoning (zrns 15 and 23B) and presumably on the recrystallized rim of an older igneous zircon (zrn 21).

The most relevant age group is represented by seven Carboniferous-Permian ages, ranging from 348 ± 3 Ma to 258 ± 2 Ma. They were measured on sub-idiomorphic (zrns 21 and 24) or rounded crystals (zrns 12, 14 and 23A) showing oscillatory or partially modified domains of zoning.

A single age referable to the Lower Devonian (416 ± 4 Ma on zrn 17) was present on one rounded crystal with an internal complex and convoluted zoning.

Two Paleoproterozoic ages were measured on one prismatic grain with a bipyramidal shape (zrn 22). The core domain, dated at 1998 ± 21 Ma, seems to refer to a partially reabsorbed inherited crystal, while the subsequent overgrowth (1885 ± 20 Ma) shows a clear magmatic oscillatory zoning.

The two oldest ages (Neoarchean 2813 ± 30 Ma and 2737 ± 29 Ma) were found on one sub-rounded grain (zrn 18) without internal recognizable textures, probably, because of the long geological history that modified it.

7. Discussion

The fine-grained sample (i.e., TTB) resulted in poorer of zircons that produced Neoarchean, Paleoproterozoic, Devonian-Carboniferous-Permian, and three predominantly Rupelian sub-concordant ages (15 ages in Figure 9b). In contrast, the medium-coarse-grained TTA sample was highly productive (i.e., 65 ages), with ages ranging from 717 ± 7 to 30 ± 1 Ma (Figure 9a).

The substantially different productivity of the datable zircons in the two samples seems to depend on grain size and alteration; the fine-grained detritus contains more alteration products in the matrix and selects lighter grains in which the zircons have a low chance to be enriched.

The U-Pb zircon ages collected in the two samples (Table 2) can be divided into three large groups: (i) Pre-Carboniferous ages; (ii) Carboniferous–Permian ages; (iii) Priabonian–Rupelian ages. The two Upper Jurassic ages and three Cretaceous ages, although poorly represented, have a relevant geological significance. In the following sections, the geological input derived from the geochronological data linked with the mineral composition of the lithic fragments is displayed.

Table 2. The U-Pb zircon concordant ages in millions of years (Ma) measured in each sample. The ages in italic font are sub-concordant with % U-Pb discordance ranging from 12% to 27%. The ages > 1.4 Ga in the TTB sample derived from the $^{206}Pb/^{207}Pb$ ratios.

Sample	Neoarchean-Paleoproterozoic Ages	Cryogenian-Ediacaran Ages	Ordovician-Devonian Ages	Carboniferous-Permian Ages	Upper Jurassic Ages	Cretaceous Ages	Priabonian-Rupelian Ages
TTA	-	717 ± 7; 640 ± 7; 614 ± 6; 606 ± 6; 573 ± 6; 535 ± 5; (506 ± 5 Cambrian)	455 ± 4; 394 ± 4; 387 ± 4	315 ± 3; 313 ± 3; 303 ± 3; 301 ± 3; 298 ± 3; 295 ± 3; 294 ± 3; 287 ± 3; 283 ± 3; 277 ± 3; 276 ± 3; 274 ± 3; 265 ± 3	157 ±2; 156 ±2	(130 ± 1 Lower Cretaceous) (78 ± 1; 67 ± 1 Upper Cretaceous)	36 ± 1; 36 ± 1; 36 ± 1; 35 ± 1; 35 ± 1; 35 ± 1; 34 ± 1; 34 ± 1; 34 ± 1; 34 ± 1; 33 ± 1; 33 ± 1; 33 ± 1; 33 ± 1; 33 ± 1; 33 ± 1; 32 ± 1; 32 ± 1; 32 ± 1; 32 ± 1; 32 ± 1; 32 ± 1; 32 ± 1; 32 ± 1; 32 ± 1; 31 ± 1; 30 ± 1; *35 ± 1; 34 ± 1; 34 ± 1; 34 ± 1; 33 ± 1; 33 ± 1, 31 ± 1*
TTB	2813 ± 30; 2737 ± 29; 1998 ± 21; 1885 ± 20		416 ± 4	348 ± 3; *338 ± 3*; 307 ± 3; 285 ± 3; 270 ± 3; 260 ± 6; 258 ± 2			*36 ± 1; 35 ± 1; 34 ± 1*

7.1. Priabonian-Rupelian Sedimentation Ages

TTF volcaniclastic sandstones are considered an expression of a syn-sedimentary volcanism mixed with scarce detritus deriving from a crystalline source of the Calabrian terranes [18,59]. Their sedimentation age still lacks a univocally definition on the biostratigraphic basis; for example, it is indicated as Late Oligocene-Early Miocene by [14,16–18] and Late Eocene-Early Oligocene by other authors [19]. Uncertainties as a result of the small number of suitable biomarkers and by various reworkings of taxa are very common in deep sea turbiditic deposits.

Newly acquired U-Pb detrital zircon data allow to clarify these uncertainties. Half of the concordant ages measured on the idiomorphic zircons with a clear magmatic oscillatory zoning presented a mean age of 33 ± 1 Ma (Figures 8 and 10a). These data, together with the abundance of fragments and single minerals of volcanic origin, indicate that the prevalent detritus was derived from an active volcanic arc in the Priabonian-Rupelian. The peak in age at 33 ± 1 Ma constrains the depositional age of TTF sandstones, confirming the oldest biostratigraphic records indicated by [19]. This sedimentation age, which emerged in the considered samples from the Lucanian Apennines, is well correlated with the sedimentation time estimated for the analogous volcaniclastic detritus of the Taveyannaz sandstones in the Western Alps (approximately 34 Ma in [60]), the Val d'Aveto-Petrignacola dated Early Oligocene [6,23], and the Ranzano formations in the Northern Apennines [7].

The records of Rupelian volcaniclastic sandstones even in the Southern Italy added a relevant geological constraint to Central Mediterranean paleogeography. The volcanic activity syn-sedimentary with TTF sandstone deposition, on the basis of these preliminary data, can be considered Rupelian in age. Consequently, relatively synchronous Priabonian-Rupelian volcanic activity along the front of the forming Apennine chain is widespread from north to south in the Western Mediterranean area,

as shown by the comparable deposition ages of the volcaniclastic sandstones incorporated in the northern and southern Apennine belt (Figure 11).

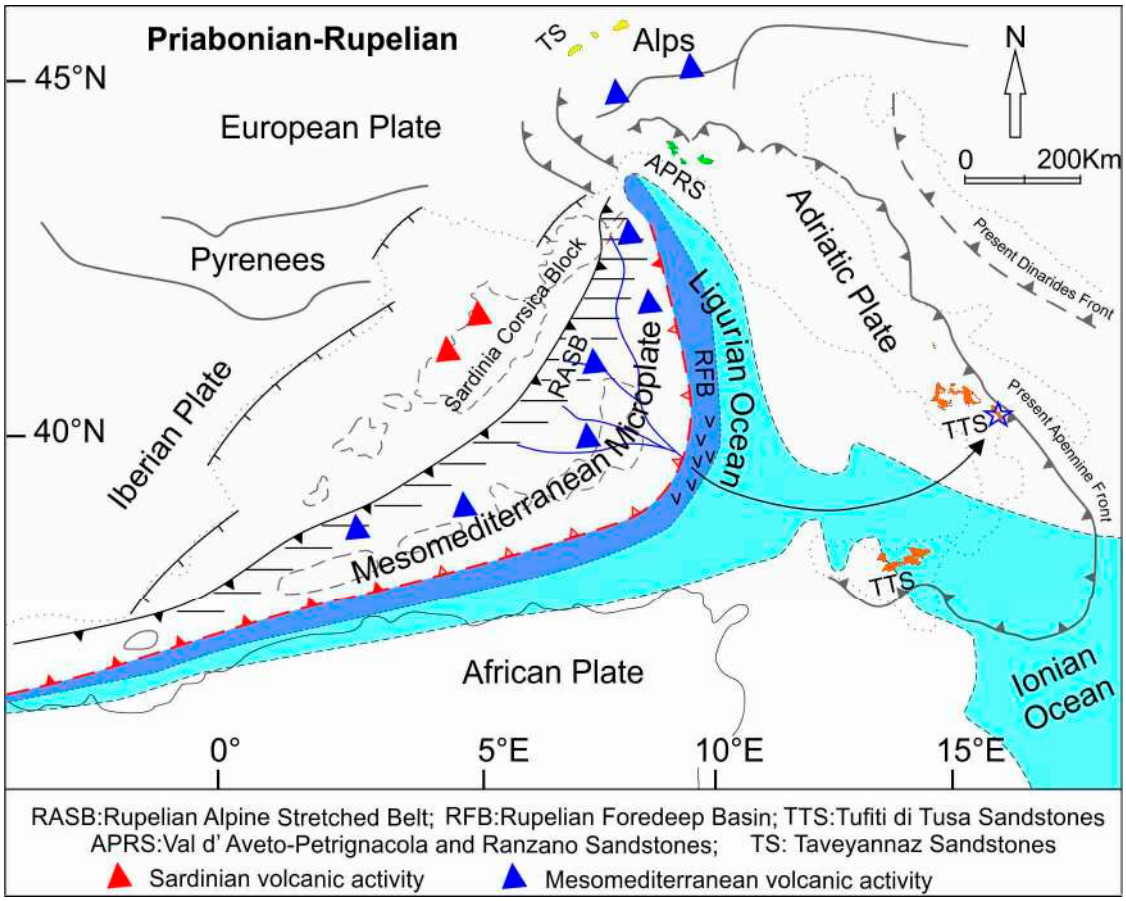

Figure 11. Redrawn paleogeographic sketch of the Western-Central Mediterranean area in the Priabonian-Rupelian age (modified from [2,20]). The Tufiti di Tusa sandstones were deposited in the Rupelian Foredeep Basin (RFB) near Mesomediterranean Microplate and far from the Sardinia-Corsica block. Symbols "vvv" represent the depositional domain of the volcaniclastic sandstones; blue star is the geographical location of the studied outcrops; blue lines indicate the drainage system. The Sardinia-Corsica volcanic activity was poor in the Priabonian–Rupelian times [6,10].

7.2. Geological History Told by Zircon Ages from the Pre-Carboniferous to the Rupelian Times

The pre-Carboniferous ages range from Neoarchean to Paleoproterozoic (around 2775 Ma and 1941 Ma, respectively), while those of Cryogenian-Ediacaran range from 717 ± 7 to 506 ± 5 Ma and those Ordovician-Silurian-Devonian from 455 ± 4 Ma to 387 ± 4 Ma (Figure 9a,b, and Figure 10b,c). Remnants of these ages are recorded in the Variscan orogen, characterized by a protracted evolution from the Neoproterozoic until the final assemblage of Pangea in the Devonian–Carboniferous period with the consumption of the Rehic Ocean and the continental collision between Laurussia and Gondwana ([61] and the references therein). Older ages (i.e., 2800 Ma and 1900 Ma) in the Variscan orogen were found in remnants produced by the gravitational collapse of the Cadomian orogeny involving the peri-Gondwanan terranes related to the West African Craton [62]. During the Carboniferous-Permian-exhumation phases, a high volume of granitoids were put in place in the Variscan orogen. In the current realm of the Mediterranean area, pieces of Variscan orogen are present from Iberia to the Anti-Atlas Mountains, and in Sardinia–Corsica (pro-part) block or are included in the Alpine chain in the Alps and the Calabria-Peloritani-Arc (Figure 1c). The relict pre-Carboniferous zircons and those of Carboniferous-Permian ages corresponding to peaks of 291 Ma and 295 Ma in

the TTA and TTB samples, respectively (Figure 10b,c), may arise from these fragments scattered in the Western–Central Mediterranean area. The inner texture of the zircons of Carboniferous–Permian ages seems related to growth in plutonic-acidic-magmatic context, such as granitoids forming large portions of the Variscan basements. Obviously, the Variscan basements that, in the Oligocene, were closer to the foredeep basins of the Apennine system, can be recognized in the Western Alps, the Sardinia Corsica (pro-part) block, and the Calabria-Peloritani-Arc (Figure 11). The sediment routing pathways are shown in Figure 11, where the detritus of the studied sandstones could be derived from pieces of continental crust belonging to the Mesomediterranean Microplate as the Calabria–Peloritani Arc that, in the Pribonian-Rupelian age was facing the foredeep basin domain (RFB in Figure 11).

During Cretaceous-Early Paleogene the eastward and southward subduction of the Tethys ocean beneath the Adriatic continental plate and the Mesomediterranean Microplate formed the Alpine Chain and successively remnants of the Alpine orogens (i.e., Alpine Corsica, Catena Costiera in Calabria, Brianzonese Zone in the Western Alps, and Ligurian-Piedmontese ophiolites) were boudinaged and passively incorporated into the hinterland of the Apennine–Maghrebian accretionary wedges [63] in the Eocene -Oligocene period (Figure 11).

In the Middle-Late Eocene, in fact, a new NW-directed Apennine-Maghrebian subduction system commenced in the Central-Western Mediterranean. During the Apennine-Maghrebian orogenesis, an intense volcanic activity took place on the hinterland terrains around 32-28 Ma, as testified by the calc-alkaline products widespread in the Alpine Chain, in the south-east of France, and in Sardinia [2,17,64]. However, the volume of subduction-related magmatism in Sardinia remained substantially very scarce from 38 to 26 Ma, reaching a peak around 22-18 Ma [2,10]. Consequently, the high volume of volcaniclastic deposits widespread in the Apennine foredeep basins cannot be related only to these volcanic centers, but more dispersed volcanos can be hypothesized to be present on the hinterland area forming the front of chain (Figure 11). The mixture of volcanic detritus with serpentinites, ophicalcites, and blue amphibole-bearing micaschists derived from ophiolitic terranes with signatures of metamorphic evolution from burial to exhumation, indicates that the remnants of the Alpine chain with volcanism relative to Oligocene were elongated from north to south in the Mediterranean area (Figure 11). In fact, according to [2,18], the Alpine chain formed a large continuum system in the Western Mediterranean area recorded in the Western Alps, testified by remnants of Alpine thrust dredged in the Tyrrhenian Sea [65] and even in deposits of the back-arc basins of Kabylie (Northern Africa) and Calabria (in Southern Italy) with signatures of subduction metamorphism [2,18].

This statement finds strict constraints in the few but significant ages measured in the zircons of TTF sandstones. In fact, the ages around 157 Ma (Figure 10b) can be connected to meta-albitite dikes dated to 152 ± 2 Ma, representing the products of a late-stage intra-oceanic magmatism injected in gabbros and basalts dated to 165 ± 3 Ma that form the oceanic Tethyan lithosphere [1,66]. The ages 67 ± 1 and 78 ± 1 Ma measured on the rims of zrn1 in the TTA sample (Figure 6b, Figure 10b) can be related, in turn, to the Alpine metamorphism dated around 65 ± 6 Ma by [67] on the zircon fringes in ophiolitic sequences of the Zermatt–Sass zone in the Western Alps. It is likely that ophiolites of similar ages were incorporated in the eastern area of Mesomediterranean Microplate overlooking the Rupelian foredeep basin (RFB in Figure 11).

The western internal domains of the foredeep basins during the Apennine tectonism were constituted by (Figure 11): (i) Remnants of Cadomian orogeny included in the Variscan chain fragments; (ii) domains of the Variscan chain formed by continental crust in which low-medium-grade metamorphites and granitoids prevail; (iii) portions of Alpine ophiolites consisting of ophicalcites, serpentinites, blue amphibole-bearing micaschists with evidences of subduction metamorphism; and (iv) andesitic calc-alkaline volcaniclastites representing a syn-sedimentary volcanism dated as Priabonian-Rupelian, likely located on the Mesomediterranean Microplate and in contrast to the volcanic activity of Sardinia with a climax in Early Miocene. All of these domains that form the Mesomediterranean Microplate were eroded by a hydrographic system that flows into the Rupelian Foredeep Basin. The western provenance direction of the detritus fits the indications derived by

paleocurrents, indicating a southern provenance due to the anticlockwise rotation of the Apennine elements [28,38–40,68].

8. Conclusions

The first U-Pb ages collected on detrital zircons and the mineralogical composition of the lithic fragments of TTF volcaniclastic sandstones from the study area in the Lucanian Apennines suggest the following deductions:

(a) The petrographic and geochemical features of the studied samples are perfectly in line with the literature data [14,28,31,37,38,59] suggesting a provenance from a magmatic arc with calc-alkaline affinity placed on a crystalline basement with a sedimentary cover;

(b) The high volume of volcanic detritus (approximately 70%) in the considered succession, with a thickness of about 60 m, shows that the maximum syn-sedimentary volcanic input in the Southern Apennines foredeep took place during the Late Priabonian–Early Rupelian as evidenced by the abundances of magmatic idiomorphic zircons with ages around 33 ± 1 Ma (Figures 8 and 10a), suggesting the true sedimentation age, for almost all the study levels. However, more volcaniclastic strata must be analyzed to extrapolate this age to the entire volcaniclastic sequence.

(c) A comparison of the established U-Pb zircon ages with those of the syn-orogenic and syn-sedimentary volcanic deposits outcropping in the Mediterranean region, shows great similarities with the ages of the volcaniclastic sandstones of the Val d'Aveto–Petrignacola and Ranzano formations in the Northern Apennine [6,8,11,23] and with those of the Taveyannaz sandstones deposited in the Northern Alpine foredeep [60].

(d) Priabonian-Rupelian volcanic activity does not correspond to the maximum climax recorded in Sardinia (around 22–18 Ma in [10]). The hinterland terranes or the Mesomediterranean Microplate facing the foredeep basins of the Apennine-Maghrebian system can be depicted as a complex structured source area formed by remnants of Cadomian terranes in the Variscan basement, consisting of granitoids and metamorphic rocks, HP-LT metamorphites, ophiolites, and Priabonian-Rupelian volcanic edifices widespread from north to south in the Western Mediterranean area.

The collected data are preliminary and represent two sedimentary episodes of volcaniclastic succession in the Southern Apennines. A future investigation of U-Pb detrital zircon ages in other volcaniclastic sandstones from Southern Apennines and Sicily would place more stringent constraints on Priabonian-Rupelian paleogeography in the Western Mediterranean area.

Supplementary Materials: The following are available online at http://www.mdpi.com/2075-163X/10/9/786/s1. Table S1: LA-ICP-MS zircon U-Pb age data for TTA and TTB Tufiti di Tusa sandstones.

Author Contributions: Conceptualization, A.F., S.G.; methodology, All Authors.; data curation, F.M., A.L.; writing—original draft preparation, S.G., F.M.; writing—review and editing, All Authors; All authors have read and agreed to the published version of the manuscript.

Funding: This research was funded by University of Bari (Italy), grant n° 00596609 ricat 01 and CARG 89/91.

Acknowledgments: We thank Pasquale Acquafredda, Nicola Mongelli and Mauro Pallara for their assistance during the instrumental analyses.

Conflicts of Interest: The authors declare no conflict of interest. The funders had no role in the design of the study, in the collection, analyses, or interpretation of data; in the writing of the manuscript, or in the decision to publish the results.

References

1. Dilek, Y.; Furnes, H. Tethyan ophiolites and Tethyan seaways. *J. Geol. Soc.* **2019**, *176*, 899–912. [CrossRef]
2. Carminati, E.; Lustrino, M.; Doglioni, C. Geodynamic evolution of the central and western Mediterranea: Tectonics vs. igneous petrology constraints. *Tectonophysics* **2012**, *579*, 173–192. [CrossRef]

3. Vitale, S.; Ciarcia, S. Tectono-stratigraphic and kinematic evolution of the southern Apennines/Calabria–Peloritani Terrane system (Italy). *Tectonophysics* **2013**, *583*, 164–182. [CrossRef]
4. De Capoa, P.; Guerrera, F.; Perrone, V.; Serrano, F.; Tramontana, M. The onset of the syn-orogenic sedimentation in the Flysch Basin of the Sicilian Maghrebids: State of the art and new biostratigraphic constraints. *Ecl. Geol. Helv.* **2000**, *93*, 65–79.
5. Guerrera, F.; Martín-Martín, M. Geodynamic events reconstructed in the Betic, Maghrebian, and Apennine chains (central-western Tethys). *Bull. Soc. Géol. Fr.* **2014**, *185*, 329–341. [CrossRef]
6. Mattioli, M.; Lustrino, M.; Ronca, S.; Bianchini, G. Alpine subduction imprint in Apennine volcaniclastic rocks.Geochemical–petrographic constraints and geodynamic implications from Early Oligocene Aveto-Petrignacola Formation (N Italy). *Lithos* **2012**, *134*, 201–220. [CrossRef]
7. Cibin, U.; Tateo, F.; Catanzariti, R.; Martelli, L.; Rio, D. Composizione, origine ed età del vulcanismo andesitico oligocenico inferiore dell'Appennino settentrionale: Le intercalazioni vulcano-derivate nella Formazione di Ranzano. *Boll. Soc. Geol. Ital.* **1998**, *117*, 569–591.
8. Malferrari, D.; Gualtieri, A.F.; Panini, F.; Fioroni, C. Oligocene-Miocene volcanism in the Apennines: Discovery and characterization of a baryte and Ba-rich phillipsite bed in the lower part of the Ranzano Formation (Reggio Emilia, Italy). *Ital. J. Geosci.* **2020**, *139*, 287–299. [CrossRef]
9. Lu, G.; Di Capua, A.; Winkler, W.; Rahn, M.; Guillong, M.; von Quadt, A.; Willett, S.D. Restoring the source-to-sink relationships in the Paleogene foreland basins in the Central and Southern Alps (Switzerland, Italy, France): A detrital zircon study approach. *Int. J. Earth Sci.* **2019**, *108*, 1817–1834. [CrossRef]
10. Lustrino, M.; Morra, V.; Fedele, L.; Franciosi, L. Beginning of the Apennine subduction system in central western Mediterranean: Constraints from Cenozoic "orogenic" magmatic activity of Sardinia, Italy. *Tectonics* **2009**, *28*, 5. [CrossRef]
11. Di Capua, A.; Vezzoli, G.; Groppelli, G. Climatic, tectonic and volcanic controls of sediment supply to an Oligocene Foredeep basin: The Val d'Aveto Formation (Northern Italian Apennines). *Sediment. Geol.* **2016**, *332*, 68–84. [CrossRef]
12. Bonardi, G.; Amore, F.O.; Ciampo, G.; de Capoa, P.; Miconnet, P. Il complesso Liguride Auct.: Stato delle conoscenze e problemi aperti dulla sur evoluzione pre-Appenninica ed i suoli rapporti con l'Arco Calabro. *Mem. Soci. Geol. Ital.* **1988**, *41*, 17–35.
13. Ciarcia, S.; Vitale, S.; Di Staso, A.; Iannace, A.; Mazzoli, S.; Torre, M. Stratigraphy and tectonics of an Internal Unit of the southern Apennines: Implications for the geodynamic evolution of the peri-Tyrrhenian mountain belt. *Terra Nova* **2009**, *21*, 88–96. [CrossRef]
14. De Capoa, P.; D'Errico, M.; Di Staso, A.; Morabito, S.; Perrone, V.; Perrotta, S. Biostratigraphic and petrographic study of the Oligocene-Lower Miocene successions of the external oceanic units in the Apennines and Sicilian Maghrebides. *Rev. Soc. Geol. Esp.* **2014**, *27*, 151–173.
15. Lentini, F.; Carbone, S. Geologia della Sicilia-geology of Sicily. *Mem. Descr. Carta Geol. Ital.* **2014**, *95*, 7–30.
16. De Capoa, P.; Di Staso, A.; Guerrera, F.; Perrone, V.; Tramontana, M. The age of the oceanic accretionary wedge and onset of continental collision in the Sicilian Maghrebian Chain. *Geodin. Acta* **2004**, *17*, 331–348. [CrossRef]
17. Martín-Martín, M.; Guerrera, F.; Tramontana, M. Geodynamic implications of the latest Chattian-Langhian central-western peri-Mediterranean volcano-sedimentary event: A review. *J. Geol.* **2020**, *128*, 29–43. [CrossRef]
18. Critelli, S. Provenance of Mesozoic to Cenozoic circum-Mediterranean sandstones in relation to tectonic setting. *Earth Sci. Rev.* **2018**, *185*, 624–648. [CrossRef]
19. Baruffini, L.; Lottaroli, F.; Torricelli, S. Integrated high-resolution stratigraphy of the lower oligocene Tusa Tuffite Formation in the Calabro-Lucano area and Sicily (southern Italy). *Riv. Ital. Paleont. Strat.* **2002**, *108*, 457–477.
20. Guerrera, F.; Martín-Martín, M.; Tramontana, M. Evolutionary geological models of the central-western peri-Mediterranean chains: A review. *Int. Geol. Rev.* **2019**, 1–22. [CrossRef]
21. Patacca, E.; Scandone, P. Geology of the Southern Apennines. *Boll. Soc. Geol. Ital.* **2007**, *7*, 75–119.
22. Molli, G.; Malavieille, J. Orogenic processes and the Corsica/Apennines geodynamic evolution: Insights from Taiwan. *Int. J. Earth Sci.* **2011**, *100*, 1207–1224. [CrossRef]

23. Malusà, M.G.; Anfinson, O.A.; Dafov, L.N.; Stockli, D.F. Tracking Adria indentation beneath the Alps by detrital zircon U-Pb geochronology: Implications for the Oligocene–Miocene dynamics of the Adriatic microplate. *Geology* **2016**, *44*, 155–158. [CrossRef]
24. Leprêtre, R.; de Lamotte, D.F.; Combier, V.; Gimeno-Vives, O.; Mohn, G.; Eschard, R. The Tell-Rif orogenic system (Morocco, Algeria, Tunisia) and the structural heritage of the southern Tethys margin. *Bulletin de la Société Géologique de France* **2018**. [CrossRef]
25. De Capoa, P.; Di Staso, A.; Guerrera, F.; Perrone, V.; Tramontana, M.; Zaghloul, M.N. The lower Miocene volcanoclastic sedimentation in the Sicilian sector of the Maghrebian Flysch Basin: Geodynamic implications. *Geodin. Acta* **2002**, *15*, 141–157. [CrossRef]
26. Guerrera, F.; Martín-Martín, M.; Raffaelli, G.; Tramontana, M. The Early Miocene "Bisciaro volcaniclastic event" (northern Apennines, Italy): A key study for the geodynamic evolution of the central-western Mediterranean. *Int. J. Earth Sci.* **2015**, *104*, 1083–1106. [CrossRef]
27. Zuppetta, A.; Russo, M.; Turco, E. Alcune osservazioni sulle Tufiti di Tusa nell'area compresa tra la Valsinni e Rocca Imperiale (confine calabro-lucano). *Boll. Soc. Geol. Ital.* **1984**, *103*, 623–627.
28. Critelli, S.; De Rosa, R.; Sonnino, M.; Zuffa, G.G. Significato dei depositi vulcanoclastici della Formazione delle Tufiti di Tusa, Miocene inferiore, Lucanìa meridionale). *Boll. Soc. Geol. Ital.* **1990**, *109*, 743–762.
29. Critelli, S.; Le Pera, E. Post-Oligocene sediment-dispersal systems and unroofing history of the Calabrian microplate, Italy. *Int. Geol. Rev.* **1998**, *40*, 609–637. [CrossRef]
30. Critelli, S. The interplay of lithospheric flexure and thrust accommodation in forming strati-graphic sequences in the southern Apennines foreland basin system, Italy. *Rend. Lincei* **1999**, *10*, 257–326. [CrossRef]
31. Perri, F.; Critelli, S.; Cavalcante, F.; Mongelli, G.; Sonnino, M.; Dominici, R.; De Rosa, R. Provenance signatures for the Miocene volcaniclastic succession of the Tufiti di Tusa Formation, southern Apennines, Italy. *Geol. Mag.* **2012**, *149*, 423–442. [CrossRef]
32. Carbone, S. Note illustrative Foglio 523 Rotondella, Carta Geologica d'Italia, 1:50.000 2013. ISPRA. Available online: https://www.isprambiente.gov.it/Media/carg/note_illustrative/523_Rotondella.pdf (accessed on 1 January 2013).
33. SGI. *Carta Geologica d'Italia, scala 1:50.000*; Foglio 523 "Rotondella": ISPRA. Available online: https://www.isprambiente.gov.it/Media/carg/523_ROTONDELLA/Foglio.html (accessed on 1 January 2012).
34. Fornelli, A.; Micheletti, F.; Langone, A.; Perrone, V. First U-Pb detrital zircon ages from Numidian sandstones in Southern Apennines (Italy): Evidences of African provenance. *Sediment. Geol.* **2015**, *320*, 19–29. [CrossRef]
35. Gallicchio, S.; Maiorano, P. Revised stratigraphy of the Serra Palazzo formation, a Miocene foredeep turbidite succession of the Southern Apennines (Italy). *Rivista Italiana di Paleontologia e Stratigrafia* **1999**, *105*, 287–302.
36. Cerone, D.; Gallicchio, S.; Moretti, M.; Tinterri, R. Vertical facies evolution of the Tufiti di Tusa Formation cropping out in the Lucanian Apennines (Southern Italy). *J. Medit. Earth Sci.* **2017**, *9*, 109–112.
37. Fornelli, A.; Piccarreta, G. Mineral and chemical provenance indicators in some early Miocene sandstones of the Southern Apennines (Italy). *Eur. J. Min.* **1997**, *9*, 433–447. [CrossRef]
38. Fornelli, A.; Gallicchio, S.; Mongelli, G.; Salvemini, A.; Summa, V.; Ventrella, N.; Zaza, S. Areniti a glaucofane nell'Appennino meridionale. *Min. Petropr. Acta* **1992**, *35*, 199–214.
39. Speranza, F.; Adamoli, L.; Maniscalco, R.; Florindo, F. Genesis and evolution of a curved mountain front: Paleomagnetic and geological evidence from the Gran Sasso range (central Apennines, Italy). *Tectonophysics* **2003**, *362*, 183–197. [CrossRef]
40. Speranza, F.; Maniscalco, R.; Grasso, M. Pattern of orogenic rotations in central–eastern Sicily: Implications for the timing of spreading in the Tyrrhenian Sea. *J. Geol. Soc.* **2003**, *160*, 183–195. [CrossRef]
41. Ingersoll, R.V.; Bullard, T.F.; Ford, R.L.; Grimm, J.P.; Pickle, J.D.; Sares, S.W. The effect of grain size on detrital modes: A test of the Gazzi-Dickinson point-counting method. *J. Sediment. Res.* **1984**, *54*, 103–116.
42. Zuffa, G.G. Unravelling hinterland and offshore palaeogeography from deep-water arenites. In *Marine Clastic Sedimentology*; Leggett, J.K., Zuffa, G.G., Eds.; Springer: Dordrecht, The Netherlands, 1987; pp. 39–61.
43. Malusà, M.G.; Garzanti, E. The Sedimentology of Detrital Thermochronology. In *Fission-Track Thermochronology and Its Application to Geology*; Malusà, M., Fitzgerald, P., Eds.; Springer: Cham, Switzerland, 2019; pp. 123–143.
44. Malusà, M.G.; Carter, A.; Limoncelli, M.; Villa, I.; Garzanti, E. Bias in detrital zircon geochronology and thermochronometry. *Chem. Geol.* **2013**, *359*, 90–170. [CrossRef]

45. Coutts, D.; Hubbard, S.M.; Matthews, W.; Bain, H.; Guest, B. Application of Large-N Detailed Max Depositional Age (MDA) Calculation to Determine Sedimentary Rates of a Deepwater Conduit. In *AAPG Annual Convention and Exhibition*; The American association of Petroleum Geologists: Tulsa, OK, USA, 2016.
46. Thomas, W.A.; Gehrels, G.E.; Sundell, K.E.; Greb, S.F.; Finzel, E.S.; Clark, R.J.; Malone, D.H.; Hampton, B.A.; Romero, M.C. Detrital zircons and sediment dispersal in the eastern Midcontinent of North America. *Geosphere* **2020**, *16*, 817–843. [CrossRef]
47. Griffin, B.J.; Joy, D.C.; Michael, J.R. A comparison of a luminescence-based VPSE and an electron-based GSED for SE and CL imaging in variable pressure SEM with conventional SE imaging. *Microsc. Microanal.* **2010**, *16*, 624–625. [CrossRef]
48. Fornelli, A.; Langone, A.; Micheletti, F.; Piccarreta, G. REE partition among zircon, orthopyroxene, amphibole and garnet in a high-grade metabasic system. *Geol. Mag.* **2018**, *155*, 1705–1726. [CrossRef]
49. Fornelli, A.; Gallicchio, S.; Micheletti, F. U-Pb detrital zircon ages and compositional features of Bifurto quartz-rich sandstones from Southern Apennines (Southern Italy): Comparison with Numidian Flysch sandstones to infer source area. *Ital. J. Geosci.* **2019**, *138*, 216–230. [CrossRef]
50. Horstwood, M.S.; Košler, J.; Gehrels, G.; Jackson, S.E.; Mclean, N.M.; Paton, C.; Bowring, J.F. Community derived standards for LA-ICP-MS U(Th) Pb geochronology–Uncertainty propagation, age interpretation and data reporting. *Geostand. Geoanal. Res.* **2016**, *40*, 311–332. [CrossRef]
51. Mueller, P.; Langone, A.; Patacci, M.; Di Giulio, A. Towards a Southern European Tethyan Palaeomargin provenance signature: Sandstone detrital modes and detrital zircon U-Pb age distribution of the Upper Cretaceous–Paleocene Monte Bignone Sandstones (Ligurian Alps, NW Italy). *Int. J. Earth Sci.* **2020**, *109*, 201–220. [CrossRef]
52. Spencer, C.J.; Kirkland, C.L.; Taylor, R.J.M. Strategies towards statistically robust interpretations in situ U-Pb zircon geochronology. *Geosci. Front.* **2016**, *7*, 581–589. [CrossRef]
53. Gehrels, G. Detrital zircon U-Pb geochronology: Current methods and new opportunities. In *Tectonics of Sedimentary Basins: Recent Advances*; Busby, C., Azor, A., Eds.; Blackwell Publishing: Oxford, UK, 2014; pp. 45–62.
54. Vermeesch, P. On the visualization of detrital age distributions. *Chem. Geol.* **2012**, *312*, 190–194. [CrossRef]
55. Dickinson, W.R. Interpreting provenance relations from detrital modes of sandstones. In *Provenance of Arenites*; Zuffa, G.C., Ed.; D. Reidel Publishing Company: Dordrecht, The Netherlands, 1985; pp. 333–362.
56. Dickinson, W.R.; Beard, L.S.; Brakenridge, G.R.; Erjavec, J.L.; Ferguson, R.C.; Inman, K.F.; Knepp, R.A.; Lindberg, F.A.; Ryberg, P.T. Provenance of North American Phanerozoic sandstones in relation to tectonic setting. *Geol. Soc. Am. Bull.* **1983**, *94*, 222–235. [CrossRef]
57. Xu, X.S.; Zhang, M.; Zhu, K.Y.; Chen, X.M.; He, Z.Y. Reverse age zonation of zircon formed by metamictisation and hydrothermal fluid leaching. *Lithos* **2012**, *150*, 256–267. [CrossRef]
58. Corfu, F.; Hanchar, J.M.; Hoskin, P.W.O.; Kinny, P. Atlas of zircon textures. In *Zircon*; Hanchar, J.M., Hoskin, P.W.O., Eds.; Reviews in Mineralogy and Geochemistry: Washington, DC, USA, 2003; pp. 469–500.
59. Critelli, S.; Muto, F.; Perri, F.; Tripodi, V. Interpreting provenance relations from sandstone detrital modes, southern Italy foreland region: Stratigraphic record of the Miocene tectonic evolution. *Mar. Pet. Geol.* **2017**, *87*, 47–59. [CrossRef]
60. Lu, G.; Winkler, W.; Rahn, M.; von Quadt, A.; Willett, S.D. Evaluating igneous sources of the Taveyannaz formation in the Central Alps by detrital zircon U–Pb age dating and geochemistry. *Swiss J. Geosci.* **2018**, *111*, 399–416. [CrossRef]
61. Arenas, R.; Martínez, S.S.; Albert, R.; Haissen, F.; Fernández-Suárez, J.; Pujol-Solà, N.; Andonaegui, P.; Díez Fernández, R.A.; Proenza, J.; Antonio Garcia-Casco, A.; et al. 100 Ma cycles of oceanic lithosphere generation in peri-Gondwana: Neoproterozoic to Devonian ophiolites from the NW African-Iberian margin of Gondwana and the Variscan Orogen. *Spec. Publ. Geol. Soc. Lond.* **2020**, *503*. [CrossRef]
62. Von Raumer, J.F.; Stampfli, G.M.; Arenas, R.; Martínez, S.S. Ediacaran to Cambrian oceanic rocks of the Gondwana margin and their tectonic interpretation. *Int. J. Earth Sci.* **2015**, *104*, 1107–1121. [CrossRef]
63. Alvarez, W.; Cocozza, T.; Wezel, F.C. Fragmentation of the Alpine orogenic belt by microplate dispersal. *Nature* **1974**, *248*, 309–314. [CrossRef]
64. Lustrino, M.; Fedele, L.; Agostini, S.; Di Vincenzo, G.; Morra, V. Eocene-Miocene igneous activity in Provence (SE France): 40Ar/39Ar data, geochemical-petrological constraints and geodynamic implications. *Lithos* **2017**, *288*, 72–90. [CrossRef]

65. Kastens, K.; Mascle, J.; Auroux, C.; Bonatti, E.; Broglia, C.; Channell, J.; Curzi, P.; Kay-Christian, E.; Glaçon, G.; Shiro hasegawa, S.; et al. ODP Leg 107 in the Tyrrhenian Sea: Insights into passive margin and back-arc basin evolution. *Geol. Soc. Am. Bull.* **1988**, *100*, 1140–1156. [CrossRef]
66. Balestro, G.; Festa, A.; Dilek, Y. Structural architecture of the Western Alpine Ophiolites, and the Jurassic seafloor spreading tectonics of the Alpine Tethys. *J. Geol. Soc.* **2019**, *176*, 913–930. [CrossRef]
67. Rebay, G.; Zanoni, D.; Langone, A.; Luoni, P.; Tiepolo, M.; Spalla, M.I. Dating of ultramafic rocks from the Western Alps ophiolites discloses Late Cretaceous subduction ages in the Zermatt-Saas Zone. *Geol. Mag.* **2018**, *155*, 298–315. [CrossRef]
68. Fornelli, A.; Gallicchio, S.; Micheletti, F.; Langone, A. U–Pb detrital zircon ages from Gorgoglione Flysch sandstones in Southern Apennines (Italy) as provenance indicators. *Geol. Mag.* **2020**. [CrossRef]